

# Monodentate versus Bidentate Carboxylate Binding in Magnesium and Calcium Proteins: What Are the Basic Principles?

Todor Dudev<sup>†</sup> and Carmay Lim<sup>\*,†,‡</sup>

*Institute of Biomedical Sciences, Academia Sinica, Taipei 11529, Taiwan, Republic of China, and  
Department of Chemistry, National Tsing Hua University, Hsinchu 300, Taiwan, Republic of China*

*Received: August 29, 2003; In Final Form: October 29, 2003*

Aspartate and glutamate side chains are unique among the 20 amino acids, in regard to possessing carboxylate groups that can bind the metal cation either monodentately (via one of the carboxylate O atoms) or bidentately (via both carboxylate O atoms). In this work, we elucidate the physical principles that determine the carboxylate-binding mode in metalloproteins by surveying the Protein Data Bank (PDB) and performing density functional and continuum dielectric calculations. The metal and its first-shell ligands are explicitly modeled and treated quantum mechanically, whereas the second-shell effects and the metal-binding site environment are implicitly taken into account. We systematically investigate the effect on the carboxylate denticity of (i) its immediate surroundings, (ii) the metal type and coordination number, (iii) the total charge of the metal complex, and (iv) the relative solvent exposure of the metal-binding site. The results suggest that the carboxylate-binding mode is determined by competition between the metal cation, on one hand, and nonacidic neighboring ligands from the metal inner or outer coordination sphere, on the other, for the second O atom of the COO<sup>−</sup> moiety. When the positive charge of the metal is reduced by coordination to negatively charged ligands, first- or second-shell ligand–carboxylate (as opposed to direct metal–carboxylate) interactions dictate the carboxylate-binding mode. In such cases, water molecules have a crucial role in stabilizing the monodentate carboxylate-binding mode of water-rich Mg complexes, whereas the peptide backbone has a role in destabilizing the monodentate carboxylate-binding mode of the “drier” and bulkier Ca complexes. Thus, by fine-tuning the respective interactions, the protein can adopt an appropriate binding-site configuration.

## 1. Introduction

Aspartate (Asp) and glutamate (Glu) side chains are among the most-common ligands that are coordinated to metal cofactors in metalloproteins.<sup>1–16</sup> They have been assigned various roles. First, they are mainly responsible for sequestering the metal cation from physiological fluids, because their interactions with the metal in a protein cavity are not only thermodynamically favorable but also are generally more favorable than those of other neutral residues or the peptide backbone.<sup>17–23</sup> In some cases, the carboxylate-binding pocket contributes to the selectivity of the metal-binding site by appropriately tuning its total charge. Thus, EF-hand Ca-binding sites that contain three Asp/Glu side chains (with a net ligand charge of −3) can selectively bind Ca(II) cations against a much higher background concentration of monovalent cations such as Na(I) and K(I).<sup>24–27</sup> Besides having a role in enhancing the affinity and/or selectivity of a protein cavity for a given metal, a first-shell Asp/Glu may also have a functional role, because it may be involved in proton shuttling in some enzymatic reactions<sup>8</sup> or it may be phosphorylated (to ~OCO–PO<sub>3</sub><sup>2−</sup>) during signal transduction processes.<sup>28,29</sup> Carboxylates that bridge two metal cations in polynuclear binding sites seem to be vital in electronically screening the metal ions, thus reducing the degree of intermetallic electronic coupling.<sup>6</sup>

Aspartate and glutamate side chains are unique among the 20 amino acids, in regard to possessing carboxylate groups that

can bind the metal cation either monodentately (via one of the carboxylate O atoms) or bidentately (with both carboxylate O atoms coordinated to the metal). The significance of the carboxylate-binding mode for metalloprotein function and/or selectivity is gradually emerging. The interconversion between monodentate and bidentate Asp/Glu in polynuclear binding sites (so-called “carboxylate shift”<sup>30</sup>) is postulated to be important in the respective catalytic process(es).<sup>6</sup> Furthermore, the binding mode of a highly conserved Glu residue (at the last position of the Ca-binding loop<sup>24</sup>) seems to have a role in discriminating between Ca(II) and Mg(II) cations in EF-hand regulatory Ca-binding proteins. *Bidentate* binding of this Glu to the Ca(II) cation is correlated with large conformational changes in the protein, which subsequently trigger a cascade of events along the signal transduction pathway.<sup>24,31</sup> In contrast, *monodentate* binding of this Glu to the Mg(II) cation has resulted in a physiologically silent protein.<sup>32</sup> The carboxylate-binding mode to a metal ion could also have a dual role in metal selectivity and catalysis, as evidenced by recent studies on the enzyme, *E. Coli* ribonuclease H1.<sup>33</sup> Bidentate binding of D70, which is a hypothesized general base in ribonuclease H1 catalysis, to the Ca(II) cation, in addition to the ligands of the native co-factor, Mg(II), enables the Ca(II) cation to displace the Mg(II) cation. It also prevents D70 from deprotonating a water nucleophile for subsequent phosphate attack, thus abolishing enzymatic activity.<sup>33</sup>

Although statistical analyses of structures deposited in the Cambridge Structure Database (CSD)<sup>34</sup> and the Protein Data Bank (PDB)<sup>35</sup> have shown that the monodentate mode is

\* Author to whom correspondence should be addressed. E-mail address: carmay@gate.sinica.edu.tw.

<sup>†</sup> Academia Sinica.

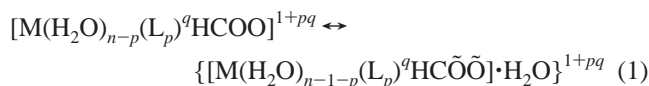
<sup>‡</sup> National Tsing Hua University.

generally more common than the bidentate mode in both small molecules and metalloproteins,<sup>36–40</sup> very little is known about the physical factors that govern the carboxylate-binding mode. Few theoretical studies have focused on carboxylate mono/bidentate equilibrium in model catalytic Zn-binding sites.<sup>41–43</sup> It has been suggested that the carboxylate group itself is “quite indifferent to its coordination mode” and its denticity is dependent mainly on other (hydrogen-bond) interactions within the complex.<sup>41</sup> Furthermore, the energy barrier between monodentate and bidentate forms seems to be small (only a few kcal/mol), allowing the zinc protein to easily adopt a functional binding site configuration at a relatively low energy cost. The role of the total charge of the complex has also been studied. In monocationic tetrahedral Zn complexes, the two carboxylate forms have been observed to be close in energy with the monodentate–bidentate equilibrium shifted in either direction, depending on the environment, whereas in neutral complexes, the monodentate mode prevails. However, several questions remain: (i) What is the role of the immediate neighbors of the carboxylates, particularly the metal-bound water molecules, in determining carboxylate denticity? (ii) Is the carboxylate-binding mode dependent on the metal type and the metal coordination number (CN)? (iii) To what extent does the solvent accessibility of the metal-binding site (the dielectric medium) affect the monodentate–bidentate equilibrium?

The aforementioned questions are addressed here, using a combined density functional theory (DFT) and continuum dielectric approach to elucidate the physical principles that determine the carboxylate-binding mode in metalloproteins. The first-shell ligands of the metal were explicitly modeled and treated quantum mechanically, whereas the second-shell effects were implicitly taken into account. As we attempt to address the aforementioned questions, not for a specific metal-binding site in a particular metalloprotein but rather for all sorts of metal-binding sites with varying degrees of solvent accessibility, the metal-binding sites were characterized with a dielectric constant ( $\epsilon$ ) in the range of 2–80. We focused mainly on magnesium and calcium proteins, given the importance of carboxylate denticity for their function and selectivity (see above discussion). However, some complexes of the Zn(II) cation (which is a representative of the transition-metal series) were also examined in addressing question (ii). We systematically investigated the effect on the carboxylate denticity of (i) its immediate surrounding, (ii) the metal type and CN, (iii) the total charge of the metal complex, and (iv) the relative solvent exposure of the metal-binding site. Furthermore, we surveyed the PDB<sup>35</sup> for Mg- and Ca-binding sites that contained inner-shell acidic (Asp and Glu) residues. On the basis of the theoretical findings, we rationalize the differences observed in the PDB between the preferred carboxylate-binding mode in magnesium and calcium proteins.

## 2. Methods

**2.1. Models Used in DFT Calculations.** Formate ( $\text{HCOO}^-$ ) was used as a model for deprotonated Asp and Glu side chains, whereas *N*-methylacetamide ( $\text{CH}_3\text{CONHCH}_3$ ) was used as a model for the backbone peptide group. In both small-molecule complexes and proteins, the Mg atom prefers hexacoordination;<sup>2,40</sup> therefore, octahedral Mg complexes were modeled. The Ca atom is more flexible, with respect to its CN, which varies from 6 to 8.<sup>2,39,40</sup> Thus, Ca complexes with CN = 6, 7, or 8 were considered here. Isomerization reactions between Mg/Ca complexes with a monodentately and bidentately bound (denoted by  $\text{HC}\ddot{\text{O}}\ddot{\text{O}}^-$ ) carboxylate were modeled:



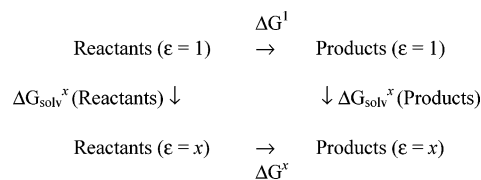
In reaction 1, M = Mg or Ca,  $n = 5-7$ ,  $p = 0-4$ ,  $q = 0$  or  $-1$ , L =  $\text{HCOO}^-$  or  $\text{CH}_3\text{CONHCH}_3$ , and the center-dot symbol ( $\cdot$ ) separates the first-shell ligands from the second-shell ones. The water molecule in the second shell is hydrogen-bonded to first-shell ligand(s). The metal CN, unless stated otherwise, was assumed to be the same when the carboxylate-binding mode was changed.

**2.2. Isomerization Free Energies in the Gas Phase.** The DFT calculations used Becke’s three-parameter hybrid method,<sup>44</sup> in conjunction with the Lee, Yang, and Parr correlation functional<sup>45</sup> and the 6-31++G(2d,2p) basis set. In previous studies, we had calibrated the B3LYP/6-31++G(2d,2p) calculations with respect to available experimental data and showed that they are well-suited for evaluating the geometries and interaction free energies of complexes between divalent cations and oxygen-/nitrogen-containing ligands.<sup>46–48</sup> Consequently, full geometry optimization for each metal complex was performed at the B3LYP/6-31++G(2d,2p) level, using the Gaussian 98 program.<sup>49</sup> Vibrational frequencies were then computed at the same level of theory/basis, to verify that each complex was at the minimum of its potential energy surface. No imaginary frequency was determined in any of the complexes. After scaling the frequencies by an empirical factor of 0.9613,<sup>50</sup> the zero-point energy (ZPE), thermal energy ( $E_T$ ), and entropy ( $S$ ) corrections were evaluated using standard statistical mechanical formulas.<sup>51</sup> The differences  $\Delta E_{\text{elec}}$ ,  $\Delta \text{ZPE}$ ,  $\Delta E_T$ , and  $\Delta S$  between the products and reactants were used to compute the isomerization free energy at  $T = 298.15$  K, according to

$$\Delta G^1 = \Delta E_{\text{elec}} + \Delta \text{ZPE} + \Delta E_T - T\Delta S \quad (2)$$

**2.3. Isomerization Free Energies in the Protein.** The reaction free energy in a given environment characterized by a dielectric constant  $\epsilon = x$  can be calculated using the thermodynamic cycle shown in Scheme 1:

### SCHEME 1



$\Delta G^1$  represents the gas-phase free energy computed using eq 2, and  $\Delta G_{\text{solv}}^x$  denotes the free energy for transferring a molecule in the gas phase to a continuous solvent medium characterized by a dielectric constant  $x$ . By solving Poisson’s equation using finite difference methods<sup>52,53</sup> to estimate  $\Delta G_{\text{solv}}^x$  (see below), the reaction free energy in an environment modeled by dielectric constant  $x$  ( $\Delta G^x$ ) can be computed from

$$\Delta G^x = \Delta G^1 + \Delta G_{\text{solv}}^x(\text{products}) - \Delta G_{\text{solv}}^x(\text{reactants}) \quad (3)$$

The continuum dielectric calculations used a  $71 \times 71 \times 71$  lattice with an initial grid spacing of 1.0 Å, and refined with a spacing of 0.25 Å. The low-dielectric region of the solute was defined as the region inaccessible to contact by a 1.4-Å-radius sphere rolling over the molecular surface. This region was assigned a dielectric constant of  $\epsilon = 2$  to account for the electronic polarizability of the solute. The molecular surface

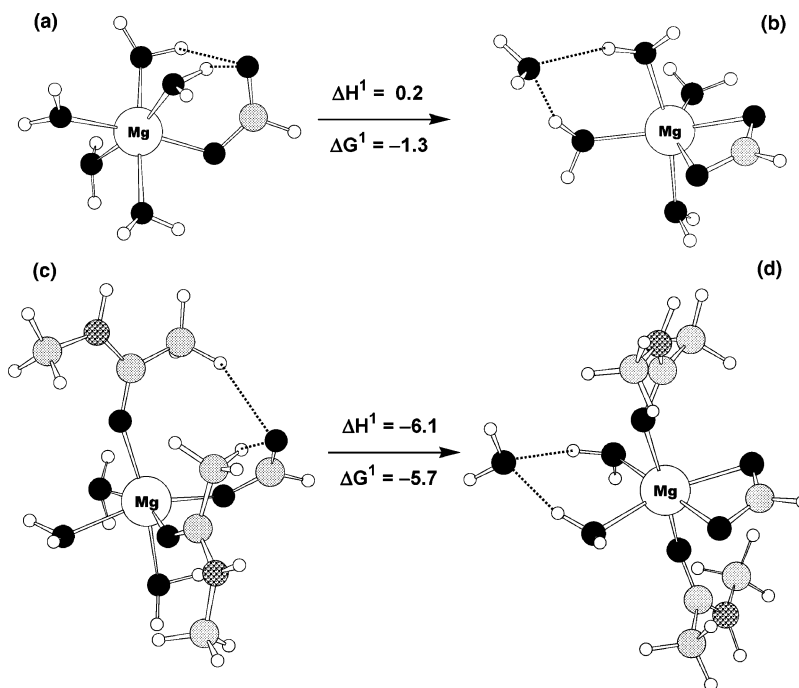


**Figure 1.** Ball-and-stick diagrams of the fully optimized complexes (a)  $[\text{Mg}(\text{H}_2\text{O})_5\text{HCOO}]^+$ , (b)  $\{[\text{Mg}(\text{H}_2\text{O})_4\text{HCOO}]^-\cdot\text{H}_2\text{O}\}^+$ , (c)  $[\text{Mg}(\text{H}_2\text{O})_3(\text{CH}_3\text{CONHCH}_3)_2\text{HCOO}]^+$ , and (d)  $\{[\text{Mg}(\text{H}_2\text{O})_2(\text{CH}_3\text{CONHCH}_3)_2\text{HCOO}]^-\cdot\text{H}_2\text{O}\}^+$ . Gas-phase enthalpies ( $\Delta H^\circ$ ) and free energies ( $\Delta G^\circ$ ) are given in kcal/mol.

was defined by effective solute radii, which were obtained by adjusting the CHARMM27<sup>54</sup> van der Waals radii to reproduce the experimental hydration free energies of the metal cations and ligands. These radii had been optimized in our previous studies<sup>3,46–48,55</sup> for B3LYP/6-31++G(2d,2p) geometries and natural bond orbital (NBO)<sup>56</sup> atomic charges:  $R_{\text{Mg}} = 1.50 \text{ \AA}$ ,  $R_{\text{Ca}} = 1.75 \text{ \AA}$ ,  $R_{\text{O}}(\text{HCOO}^-) = 1.65 \text{ \AA}$ ,  $R_{\text{O}}(\text{H}_2\text{O}) = 1.69 \text{ \AA}$ ,  $R_{\text{O}}(\text{CH}_3\text{CONHCH}_3) = 1.79 \text{ \AA}$ ,  $R_{\text{N}} = 1.70 \text{ \AA}$ ,  $R_{\text{C}} = 1.90 \text{ \AA}$ ,  $R_{\text{H}}(\text{H}_2\text{O}) = 1.0$ ,  $R_{\text{H}}(\text{C}, \text{N}) = 1.468 \text{ \AA}$ . Thus, Poisson's equation was solved with  $\epsilon = 1, 2, 4, 10$ , or  $80$ . The difference between the computed electrostatic potentials in a given dielectric medium ( $\epsilon = x$ ) and in the gas phase ( $\epsilon = 1$ ) yielded the solvation free energy  $\Delta G_{\text{sol}}^x$  of the metal complex.

**2.4. Database Survey.** The PDB<sup>35</sup> was surveyed for  $<2.5 \text{ \AA}$  X-ray and NMR structures of Mg(II) and Ca(II) proteins that contained at least one Asp or Glu in the metal first coordination shell. Polynuclear metal-binding sites and sites that contain other nonaqua/non-amino acid ligands such as phosphate or sulfate groups were excluded from the survey. Thus, only mononuclear binding sites in which Mg(II) and Ca(II) cations are coordinated respectively to six and seven amino acids or water molecules in the first shell (the most-common configurations for the two metals in protein binding sites<sup>2</sup>) were considered. The protein sequences were aligned using the Modeler 4 program<sup>57</sup> and those with a sequence identity higher than 30% were considered to belong to the same protein family. Only one representative from each protein family—namely, the structure solved at the highest resolution—was included in the survey. Analysis of high-resolution X-ray structures of small metal complexes in the CSD has shown that the bond distances between the metal and first-shell carboxylate O atoms do not exceed 2.4 and 2.7  $\text{\AA}$  in Mg(II) and Ca(II) complexes, respectively.<sup>36–40</sup> To account for the lower resolution of some of the PDB structures, slightly larger cutoffs of 2.6  $\text{\AA}$  for Mg(II) complexes and 2.9  $\text{\AA}$  for Ca(II) complexes were used to determine monodentate and bidentate carboxylate structures. Carboxylates with only one of the Mg/Ca–O bond distances falling within the respective cutoffs were

considered as monodentate, whereas those with both Mg/Ca–O bond distances within the chosen cutoffs were treated as bidentate.

### 3. Results

**3.1. Role of Carboxylate Immediate Neighbors.** Hexacoordinated Mg complexes, each containing five water molecules and a single formate (Figure 1a,b), were modeled. The metal-free O atom of the monodentate formate is engaged in hydrogen-bond formation with two of its neighboring water molecules (Figure 1a). To retain the metal coordination of CN = 6 in the bidentate structure, a water molecule was placed in the metal outer-coordination sphere, where it is hydrogen-bonded to first-shell water ligands (Figure 1b). The gas-phase thermodynamic parameters for the isomerization of  $[\text{Mg}(\text{H}_2\text{O})_5\text{HCOO}]^+$  (Figure 1a) to  $\{[\text{Mg}(\text{H}_2\text{O})_4\text{HCOO}]^-\cdot\text{H}_2\text{O}\}^+$  (Figure 1b) shows that the two structures are almost isoenergetic ( $\Delta H^\circ = 0.2 \text{ kcal/mol}$ ). However, the freeing of a metal-bound water molecule to the second shell upon bidentate binding results in a favorable entropic term ( $T\Delta S^\circ = 1.5 \text{ kcal/mol}$ ); hence, the gas-phase free energy of the bidentate complex is slightly more favorable than that of its monodentate counterpart ( $\Delta G^\circ = -1.3 \text{ kcal/mol}$ ). Because of the small  $|\Delta H^\circ|$  and  $|T\Delta S^\circ|$  terms, additional second-shell interactions that stabilize the metal-free carboxylate O atom may tip the equilibrium in favor of the monodentate structure (see Discussion section).

To assess the degree to which hydrogen-bonding interactions of the metal-free carboxylate O atom with neighboring ligands contribute to the stability of the monodentate complex, the two water molecules that were hydrogen-bonded to the metal-free carboxylate O atom were substituted with two  $\text{CH}_3\text{CONHCH}_3$  molecules. The *N*-methylacetamide methyl groups, because of the low H–C bond polarity, are poorer hydrogen-bond acceptors than the water H–O groups. The hydrogen-bonding interactions between the metal-free carboxylate O atom and the methyl H atoms (Figure 1c) are weaker than those between the metal-free carboxylate O atom and the water H atoms (Figure 1a);



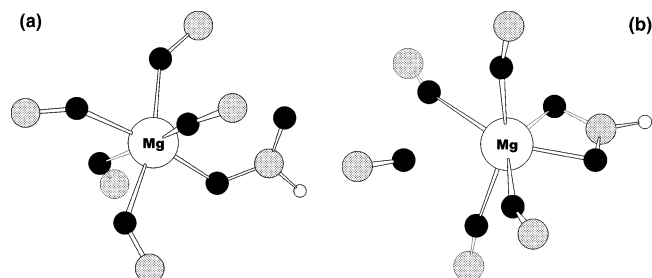


**Figure 2.** Ball-and-stick diagrams of the (a) initial and (b) final structure of the  $[\text{Mg}(\text{CO})_5\text{HCOO}]^+$  complex.

therefore, these interactions do not stabilize the monodentate complex as much as those between the metal-free carboxylate O atom and water H atoms, as evidenced by a negative  $\Delta H^\ddagger$  value ( $-6.1$  kcal/mol). In contrast to the first reaction, the isomerization of  $[\text{Mg}(\text{H}_2\text{O})_3(\text{CH}_3\text{CONHCH}_3)_2\text{HCOO}]^+$  (Figure 1c) to  $\{[\text{Mg}(\text{H}_2\text{O})_2(\text{CH}_3\text{CONHCH}_3)_2\text{HC}\ddot{\text{O}}\ddot{\text{O}}]\cdot\text{H}_2\text{O}\}^+$  (Figure 1d) is enthalpy-driven, because  $\Delta G^\ddagger = -5.7$  kcal/mol. In this case, the bidentate form is favored by the loss of hydrogen-bonding interactions between the metal-free carboxylate O atom and its neighbors, which had stabilized the monodentate complex. The observed stability of the hydrogen-bonded monodentate carboxylate–water ( $\text{HCOO}^- \cdots \text{H}_2\text{O}$ ) motif in Mg- and Mn-binding sites has also been reported by Glusker and co-workers.<sup>11,58</sup>

To verify the importance of hydrogen-bonding interactions of the metal-free carboxylate O atom in stabilizing the monodentate complex, we modeled a hypothetical Mg-binding site that consisted of a monodentately bound formate and five CO ligands, which cannot form any hydrogen bonds with the metal-free carboxylate O atom. The initial structure of this complex, shown in Figure 2a, was determined to be unstable, because it spontaneously isomerized to the bidentate complex (Figure 2b), with one of the CO ligands being transferred to the metal outer sphere. Altogether, the results shown in Figures 1 and 2 imply that the stability of the monodentate complex is dependent on creating favorable interactions between the metal-free carboxylate O atom and its immediate neighbors from either the inner or outer shell of the metal. They also imply that bidentate coordination could be favored over monodentate coordination by “negative” design; i.e., by preventing interactions that could stabilize the metal-free carboxylate O atom.

**3.2. Role of Metal Cation.** To examine how the metal affects the carboxylate coordination mode, the thermodynamic parameters for the isomerization reactions of octahedral Ca, Mg, and Zn (as a representative of the transition-metal series) complexes that contain water ligands and a single  $\text{HCOO}^-$  or  $\text{HC}\ddot{\text{O}}\ddot{\text{O}}^-$  were computed (Table 1). In going from Ca complexes to Mg complexes to Zn complexes, the gas-phase enthalpy and free energy ( $\Delta G^\ddagger$ ) each become more favorable. The free energy is correlated with the difference between the charge transferred to the metal cation in the bidentate and monodentate structures ( $\Delta\Delta q$ ), which becomes more positive in the following order:  $\Delta\Delta q(\text{Ca}) < \Delta\Delta q(\text{Mg}) < \Delta\Delta q(\text{Zn})$  (see Table 1). Hence, the greater the charge transfer to the “bidentately bound” metal,

relative to the respective “monodentately bound” metal, the more stable the bidentate complex. These results imply that different metal cations will affect the carboxylate-binding mode to a different extent: Metal cations, such as  $\text{Zn}(\text{II})$ , that can accept more charge from a bidentately bound carboxylate, relative to a monodentately bound carboxylate, than corresponding dications, such as  $\text{Mg}(\text{II})$  or  $\text{Ca}(\text{II})$ , will prefer to bind the carboxylate group bidentately rather than monodentately. Compared to divalent cations, trivalent cations that can accept more charge from a bidentately bound carboxylate, relative to a monodentately bound carboxylate, will also prefer to bind the carboxylate group bidentately, as evidenced by the finding in other works that the  $\text{La}^{3+}$  cation prefers binding a bidentate carboxylate more than the divalent  $\text{Ca}^{2+}$  cation does.<sup>59</sup>

**3.3. Role of Metal Cation CN.** 3.3.1. Rigid Binding Sites. The  $\text{Ca}(\text{II})$  cation, unlike the  $\text{Mg}(\text{II})$  cation, adopts different CNs ( $\text{CN} = 6\text{--}8$ ; see Methods section), and, thus, is an appropriate target for studying the effect of the metal CN on the carboxylate monodentate/bidentate equilibrium. Zinc is again included here, because it is found to adopt CNs in the range of 4–6 in proteins.<sup>2,39,40</sup> Thus, tetra-, penta-, and hexacoordinated Zn complexes, as well as hexa-, hepta-, and octacoordinated Ca clusters were modeled, in accordance with empirical observations.<sup>2,39,40</sup> We first consider monodentate/bidentate isomerization in rigid binding sites where the metal adopts the same CN, regardless of the carboxylate-binding mode. As the CN of the metal increases, the  $\Delta H^\ddagger$  value becomes more favorable (more negative) for the Zn complexes (Figure 3) and less unfavorable (less positive) for the Ca complexes (Figure 4). Because the gas-phase entropic change is positive, which is due to the freeing of a metal-bound water molecule into the second shell upon bidentate binding, the gas-phase isomerization free energy  $\Delta G^\ddagger$  becomes more favorable as the CN increases:  $\Delta G^\ddagger$  decreases from 1.0 kcal/mol to  $-2.2$  kcal/mol and then to  $-3.4$  kcal/mol when the Zn CN is increased from 4 to 5 and then to 6, respectively, whereas it decreases from 1.1 kcal/mol to  $-0.7$  kcal/mol and then to  $-1.5$  kcal/mol when the Ca CN is increased from 6 to 7 and then to 8, respectively.

These findings can be rationalized mainly in terms of steric crowding of the ligands around the metal. As the number of ligands coordinated to the metal increases, steric repulsion among the ligands increases; consequently, the relative size of the ligands becomes important. In comparing the two competing entities—the bidentate  $\text{HC}\ddot{\text{O}}\ddot{\text{O}}^-$  on one hand, and the “hydrogen-bonded”  $\text{HCOO}^- \cdots \text{H}_2\text{O}$  motif<sup>40</sup> on the other hand—the former occupies less volume and is less space-demanding than the latter: The average distance between the two metal-bound  $\text{HC}\ddot{\text{O}}\ddot{\text{O}}^-$  O atoms is 2.20 Å in the  $\text{Zn}(\text{II})$  structures in Figure 3 and 2.22 Å in the  $\text{Ca}(\text{II})$  structures in Figure 4, whereas the average distance between the metal-bound  $\text{O}(\text{HCOO}^-)$  and  $\text{O}(\text{H}_2\text{O})$  in the “hydrogen-bonded motif” is 3.05 Å in the Zn clusters and 3.18 Å in the Ca clusters. Thus, larger metal complexes with higher CNs seem to favor bidentate rather than monodentate carboxylate binding. Consistent with this conclusion, octacoordinated La water–carboxylate complexes are

**TABLE 1: Gas-Phase Enthalpy ( $\Delta H^\ddagger$ ),  $T\Delta S^\ddagger$  Value, and Free Energy ( $\Delta G^\ddagger$ ) for Monodentate–Bidentate Carboxylate Isomerization in Hexacoordinated  $\text{Ca}(\text{II})$ ,  $\text{Mg}(\text{II})$ , and  $\text{Zn}(\text{II})$  Complexes**

	reaction	$\Delta H^\ddagger$ (kcal/mol)	$T\Delta S^\ddagger$ (kcal/mol)	$\Delta G^\ddagger$ (kcal/mol)	$\Delta\Delta q^a$ (e)
1	$[\text{Ca}(\text{H}_2\text{O})_5\text{HCOO}]^+ \rightarrow \{[\text{Ca}(\text{H}_2\text{O})_4\text{HC}\ddot{\text{O}}\ddot{\text{O}}]\cdot\text{H}_2\text{O}\}^+$	1.5	0.4	1.1	$-0.006$
2	$[\text{Mg}(\text{H}_2\text{O})_5\text{HCOO}]^+ \rightarrow \{[\text{Mg}(\text{H}_2\text{O})_4\text{HC}\ddot{\text{O}}\ddot{\text{O}}]\cdot\text{H}_2\text{O}\}^+$	0.2	1.5	$-1.3$	0.005
3	$[\text{Zn}(\text{H}_2\text{O})_5\text{HCOO}]^+ \rightarrow \{[\text{Zn}(\text{H}_2\text{O})_4\text{HC}\ddot{\text{O}}\ddot{\text{O}}]\cdot\text{H}_2\text{O}\}^+$	$-1.5$	1.9	$-3.4$	0.028

<sup>a</sup>  $\Delta\Delta q$  is the difference between the charge transferred to the metal cation in the bidentate  $|\Delta q_M^{\text{bi}}|$  and monodentate structures  $|\Delta q_M^{\text{mono}}|$ ; i.e.,  $\Delta\Delta q = |\Delta q_M^{\text{bi}}| - |\Delta q_M^{\text{mono}}|$ , using NBO atomic charges.

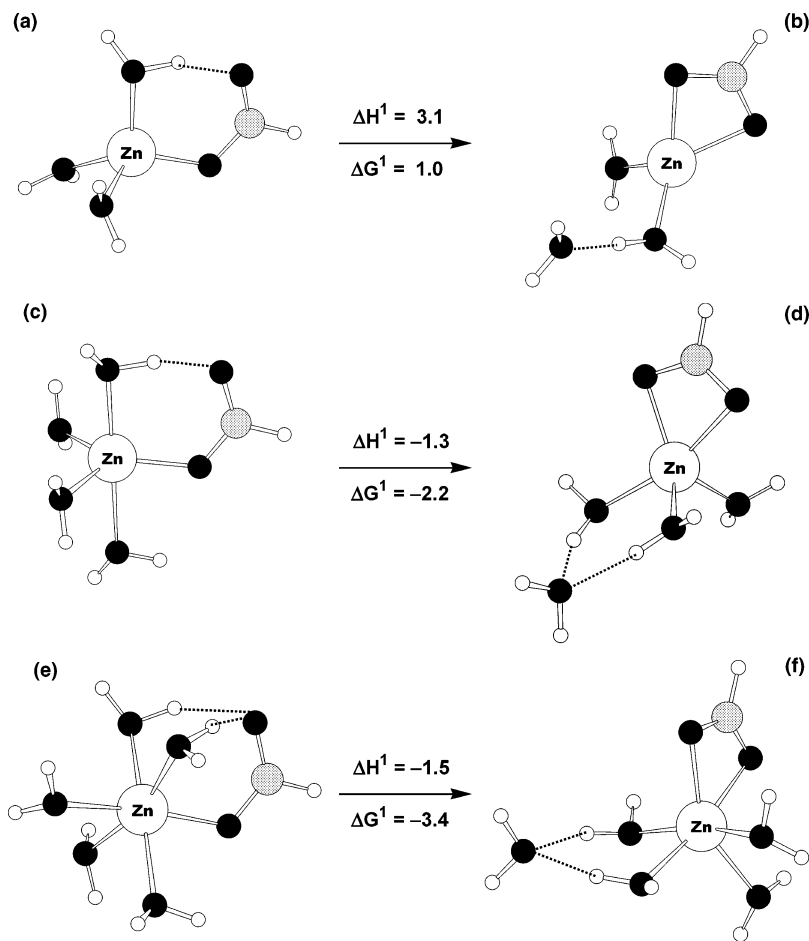


**Figure 3.** Ball-and-stick diagram of the fully optimized complexes (a)  $[\text{Zn}(\text{H}_2\text{O})_3\text{HCOO}]^+$ , (b)  $\{[\text{Zn}(\text{H}_2\text{O})_2\text{HC}(\text{O})\ddot{\text{O}}]\cdot\text{H}_2\text{O}\}^+$ , (c)  $[\text{Zn}(\text{H}_2\text{O})_4\text{HCOO}]^+$ , (d)  $\{[\text{Zn}(\text{H}_2\text{O})_3\text{HC}(\text{O})\ddot{\text{O}}]\cdot\text{H}_2\text{O}\}^+$ , (e)  $[\text{Zn}(\text{H}_2\text{O})_5\text{HCOO}]^+$ , and (f)  $\{[\text{Zn}(\text{H}_2\text{O})_4\text{HC}(\text{O})\ddot{\text{O}}]\cdot\text{H}_2\text{O}\}^+$ . Gas-phase enthalpies ( $\Delta H^1$ ) and free energies ( $\Delta G^1$ ) are given in kcal/mol.

determined to have a greater preference for the bidentate carboxylate-binding mode than the respective heptacoordinated La complexes.<sup>59</sup>

**3.3.2. Flexible Binding Sites.** We next consider monodentate/bidentate isomerization in flexible metal binding sites where the metal can expand its CN to accommodate an extra M–O bond; i.e.,



where  $\text{M} = \text{Zn}$  or  $\text{Ca}$ ,  $n = 3, 4$ , or  $6$ , and the metal CN in the bidentate complex ( $n + 2$ ) is one greater than that in the monodentate complex ( $n + 1$ ). Surprisingly, even though no metal-bound water molecules are released in the process, the gas-phase entropic changes for reaction 4 are favorable (positive) and comparable to those where a metal-bound water molecule is released to the second shell. Comparing the  $\Delta H^1$  and  $\Delta G^1$  values for reaction 4 with those for the respective rigid binding sites in Figures 3 and 4 reveals that the former values are less favorable (more positive) than the latter. Thus,  $\Delta H^1$  and  $\Delta G^1$  values for  $[\text{Zn}(\text{H}_2\text{O})_3\text{HCOO}]^+ \rightarrow [\text{Zn}(\text{H}_2\text{O})_3\text{HC}(\text{O})\ddot{\text{O}}]^+$  (the “4 → 5” reaction; see Figure 5a and b) are 4.4 and 3.2 kcal/mol, respectively, whereas the respective numbers for  $[\text{Zn}(\text{H}_2\text{O})_3\text{HCOO}]^+ \leftrightarrow \{[\text{Zn}(\text{H}_2\text{O})_2\text{HC}(\text{O})\ddot{\text{O}}]\cdot\text{H}_2\text{O}\}^+$  (the “4 → 4” reaction; see Figure 3a and b) are 3.1 and 1.0 kcal/mol. The same trend is observed for the next two reactions in Figure 5: the  $\Delta H^1$  and  $\Delta G^1$  values for the Zn “5 → 6” reaction shown in Figure 5c and d are 2.4 and 0.8 kcal/mol, whereas those for the Zn “5 → 5” reaction shown in Figure 3c and d are −1.3 and −2.2

kcal/mol, respectively. In analogy, the  $\Delta G^1$  values for the Ca “7 → 8” reaction in Figure 5e and f are 2.3 and 0.2 kcal/mol, whereas those for the Ca “7 → 7” reaction in Figure 4c and d are 1.3 and −0.7 kcal/mol.

The  $\Delta H^1$  and, thus,  $\Delta G^1$  values become more unfavorable when the metal expands its CN to accommodate an extra M–O bond rather than releasing a metal-bound water molecule because of two factors. First, the bidentate complexes in Figure 5 are destabilized, relative to their counterparts in Figure 3 or 4, which have one less metal ligand (water molecule) and, therefore, are less crowded. Second, as the CN of the metal increases, the M–O bond distances become longer, which, in turn, weakens the interactions (electrostatic, polarization, and charge transfer) between the metal cation and  $\text{HC}(\text{O})\ddot{\text{O}}^-$ .<sup>60</sup> The results thus imply that releasing a metal-bound water molecule upon monodentate → bidentate isomerization, which allows the metal to preserve its initial coordination geometry, favors bidentate carboxylate binding.

**3.4. Effect of Complex Total Charge.** **3.4.1. Magnesium Complexes.** To explore how the net charge  $Q$  of the metal complex affects the carboxylate coordination mode, the thermodynamic parameters for the isomerization reactions of Mg–carboxylate complexes with  $Q = +1$  (Figure 1a and b), 0 (Figure 6a and b), and −1 (Figure 6c and d) were computed. The reaction enthalpies  $\Delta H^1$  become more unfavorable (more positive) as more formates are bound to the Mg(II) cation:  $\Delta H^1 = 0.2, 2.8$ , and 4.4 kcal/mol for the monoformate, diformate, and triformate complexes, respectively. The  $\Delta G^1$  free energy for isomerization of the diformate or triformate complex (2.3

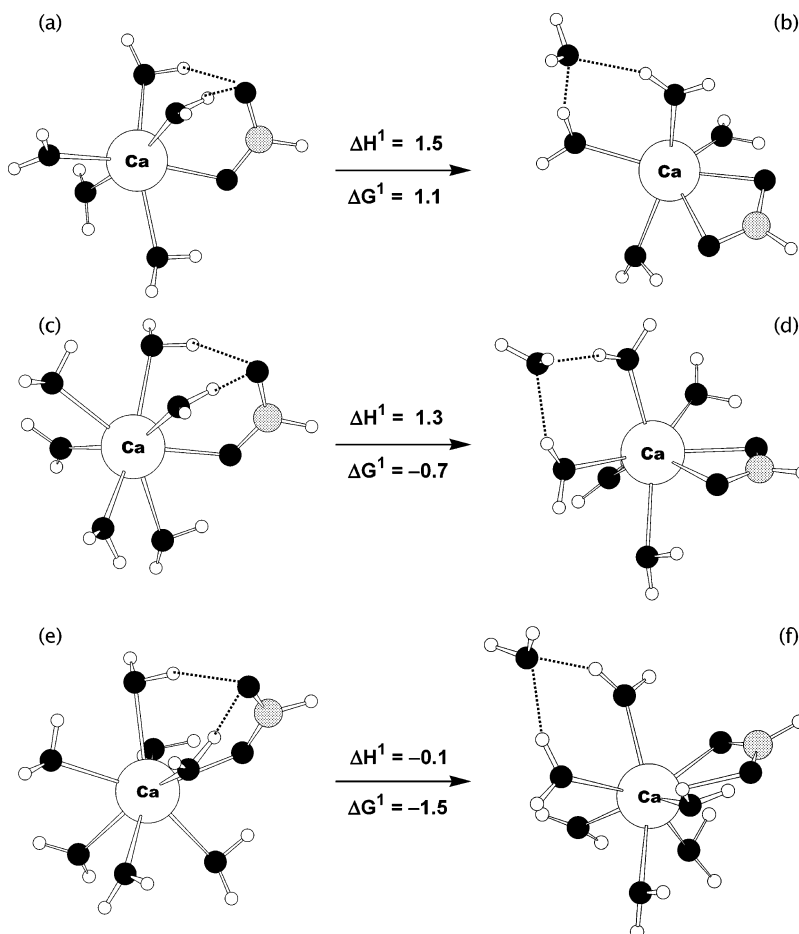
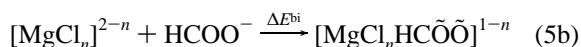
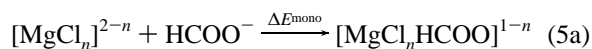


**Figure 4.** Ball-and-stick diagrams of the fully optimized complexes (a)  $[\text{Ca}(\text{H}_2\text{O})_5\text{HCOO}]^+$ , (b)  $\{[\text{Ca}(\text{H}_2\text{O})_4\text{HCOO}]\cdot\text{H}_2\text{O}\}^+$ , (c)  $[\text{Ca}(\text{H}_2\text{O})_6\text{HCOO}]^+$ , (d)  $\{[\text{Ca}(\text{H}_2\text{O})_5\text{HCOO}]\cdot\text{H}_2\text{O}\}^+$ , (e)  $[\text{Ca}(\text{H}_2\text{O})_7\text{HCOO}]^+$ , and (f)  $\{[\text{Ca}(\text{H}_2\text{O})_6\text{HCOO}]\cdot\text{H}_2\text{O}\}^+$ . Gas-phase enthalpies ( $\Delta H^1$ ) and free energies ( $\Delta G^1$ ) are given in kcal/mol.

or 2.5 kcal/mol) are more unfavorable than that for isomerization of the monoformate complex ( $-1.3$  kcal/mol). This implies that reducing the net positive charge of the metal complex favors monodentate carboxylate binding. This conclusion is in accord with previous theoretical findings on tetrahedral Zn(II) complexes, where a bidentate  $\rightarrow$  monodentate switch occurred when the net charge of the complex was reduced from  $+1$  to  $0$ .<sup>41</sup>

Why does the carboxylate-binding mode switch when the net charge of the complex changes? To answer this question, we attempted to isolate the effect of the total charge on the carboxylate-binding geometry, using waterless Mg complexes to avoid unwanted ligand–ligand interactions. The net charge was manipulated by changing the number of Mg-bound  $\text{Cl}^-$  anions, and the carboxylate binding energies ( $\Delta E$ ) were evaluated for the following reactions:



where  $n = 0, 1, 2$ . For the monodentate structures, the  $\text{Mg}-\hat{\text{O}}-\text{C}$  angle was fixed at  $130^\circ$  (the average value in fully optimized Mg(II)-formate–water structures), whereas the other internal coordinates were fully optimized. The constraint on the  $\text{Mg}-\hat{\text{O}}-\text{C}$  angle was imposed to prevent the monodentate formate from becoming bidentately bound in the absence of water molecules. No restrictions were imposed for the bidentate structures, which were fully optimized.

Both bidentate ( $\Delta E_{\text{bi}}$ ) and monodentate ( $\Delta E_{\text{mono}}$ ) carboxylate binding energies decrease in magnitude as the total charge of the complex becomes less positive/more negative. This finding can be rationalized by the decrease in the positive charge on magnesium,  $q_{\text{Mg}}$ , as the number of negatively charged  $\text{Cl}^-$  anions bound to the Mg atom increases (Table 2), which, in turn, weakens the  $\text{Mg}-\text{HCOO}^-$  charge–charge interaction.

Although the  $\Delta E_{\text{bi}}$  energies are more favorable than the respective  $\Delta E_{\text{mono}}$  energies, their difference ( $\Delta E_{\text{mono}} - \Delta E_{\text{bi}}$ ) decreases as the total charge of the complex decreases from  $+1$  to  $0$  and then to  $-1$  (see Table 2). This is because  $\Delta E_{\text{bi}}$  decays faster than  $\Delta E_{\text{mono}}$ , as shown in Figure 7. As the net positive charge of the complex decreases, the partial positive charge on the Mg atom also decreases, resulting in a greater loss of charge–charge interactions when *both* carboxylate O atoms interact with the Mg(II) cation than when only one carboxylate O atom coordinates to the metal. As the monodentate and bidentate complex energies become closer with decreasing positive charge of the complex, the role of other factors, such as interligand interactions, in determining the relative stability of the monodentate versus bidentate complexes increases.

**3.4.2. Calcium Complexes.** To determine if the effects of the net charge of the metal complex on the carboxylate coordination mode also apply to Ca–carboxylate complexes, the thermodynamic parameters for the isomerization reactions of heptacoordinated Ca–carboxylate complexes with a net charge of  $+1$  (see Figure 4c and d),  $0$  (Figure 8a and b), and  $-1$  (Figure 8c and d) were computed. The trends in the changes of the

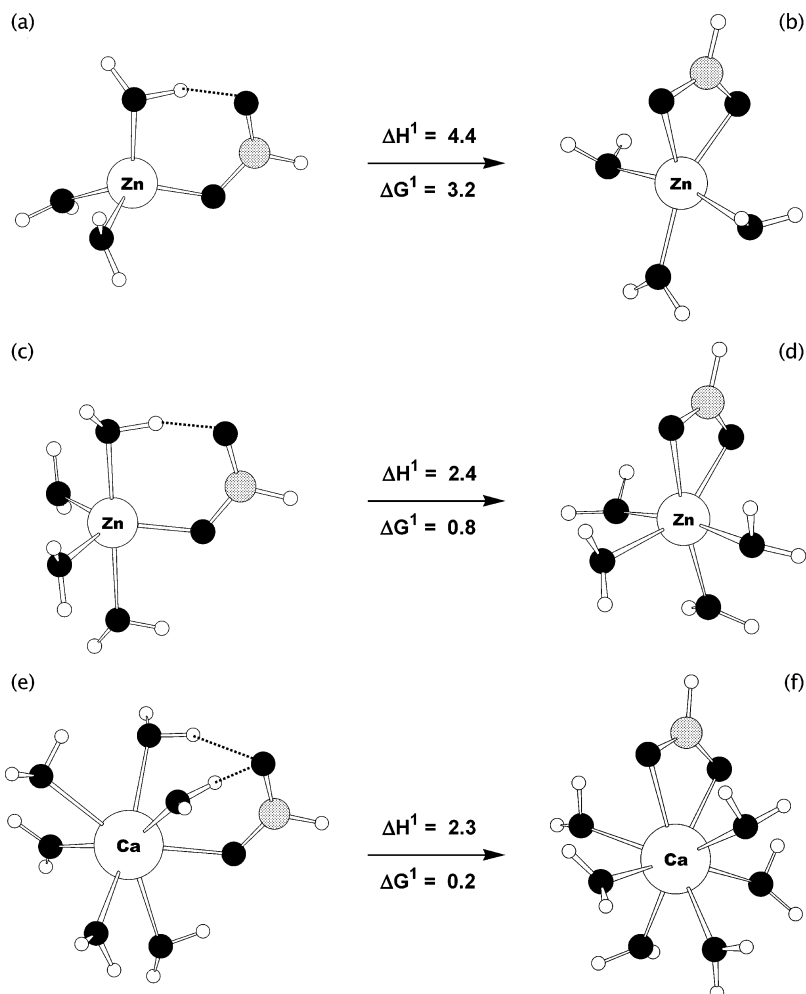


**Figure 5.** Ball-and-stick diagrams of the fully optimized complexes (a)  $[\text{Zn}(\text{H}_2\text{O})_3\text{HCOO}]^+$ , (b)  $[\text{Zn}(\text{H}_2\text{O})_3\text{HCOO}]^+$ , (c)  $[\text{Zn}(\text{H}_2\text{O})_4\text{HCOO}]^+$ , (d)  $[\text{Zn}(\text{H}_2\text{O})_4\text{HCOO}]^+$ , (e)  $[\text{Ca}(\text{H}_2\text{O})_6\text{HCOO}]^+$ , and (f)  $[\text{Ca}(\text{H}_2\text{O})_6\text{HCOO}]^+$ . Gas-phase enthalpies ( $\Delta H^1$ ) and free energies ( $\Delta G^1$ ) are given in kcal/mol.

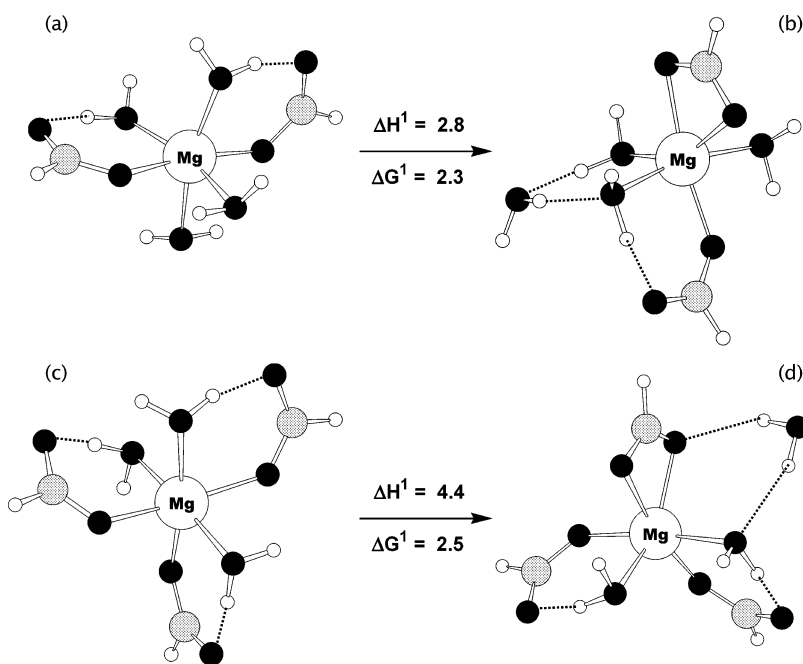


**Figure 6.** Ball-and-stick diagrams of the fully optimized complexes (a)  $[\text{Mg}(\text{H}_2\text{O})_4(\text{HCOO})_2]^0$ , (b)  $\{[\text{Mg}(\text{H}_2\text{O})_3(\text{HCOO})_2\text{HCOO}]\cdot\text{H}_2\text{O}\}^0$ , (c)  $[\text{Mg}(\text{H}_2\text{O})_3(\text{HCOO})_3]^-$ , and (d)  $\{[\text{Mg}(\text{H}_2\text{O})_2(\text{HCOO})_2\text{HCOO}]\cdot\text{H}_2\text{O}\}^-$ . Gas-phase enthalpies ( $\Delta H^1$ ) and free energies ( $\Delta G^1$ ) are given in kcal/mol.

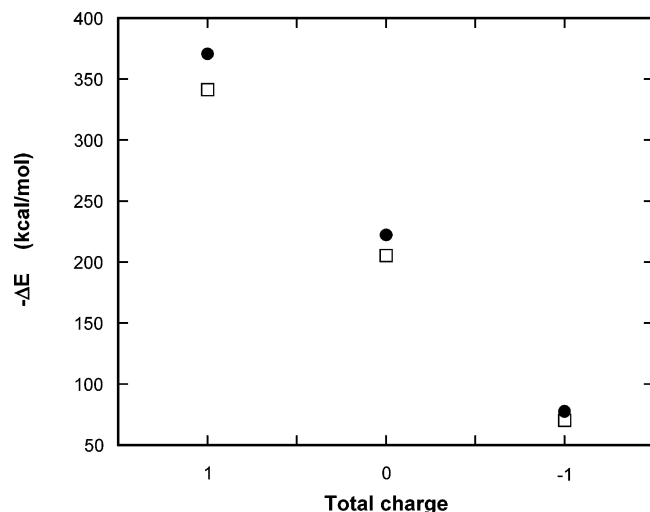
thermodynamic quantities for Ca complexes are similar to those for their Mg counterparts (see aforementioned discussion): The  $\Delta H^1$  values become more unfavorable (more positive) as the

total charge of the Ca complex goes from +1 to 0 and then to -1. Furthermore, a switch in the formate-binding mode from bidentate to monodentate occurs when the overall charge



**TABLE 2: Binding Energies ( $\Delta E$ ) for  $[\text{MgCl}_n]^{2-n} + \text{HCOO}^- \rightarrow [\text{MgCl}_n(\text{HCOO}^-)]^{2-n}$  ( $n = 0, 1, 2$ )**

complex	net charge, $Q$ (e)	$q_{\text{Mg}}$ (e)	$\Delta E$ (kcal/mol)	$\Delta E^{\text{mono}} - \Delta E^{\text{bi}}$ (kcal/mol)
$[\text{Mg}(\text{HCOO})]^+$	+1	1.784	-341.4	29.3
$[\text{Mg}(\text{HC}\ddot{\text{O}}\ddot{\text{O}})]^+$	+1	1.753	-370.7	0
$[\text{MgCl}(\text{HCOO})]^0$	0	1.737	-205.5	16.7
$[\text{MgCl}(\text{HC}\ddot{\text{O}}\ddot{\text{O}})]^0$	0	1.705	-222.2	0
$[\text{MgCl}_2(\text{HCOO})]^-$	-1	1.688	-70.4	7.4
$[\text{MgCl}_2(\text{HC}\ddot{\text{O}}\ddot{\text{O}})]^-$	-1	1.663	-77.8	0

**Figure 7.** Dependence between the formation energy ( $\Delta E$ ) and the total charge in (□) monodentate  $\text{Mg-Cl/HCOO}^-$  and (●) bidentate  $\text{Mg-Cl/HC}\ddot{\text{O}}\ddot{\text{O}}^-$  complexes.

changes from +1 to 0 ( $\Delta G^1$  changes from  $-0.7$  to  $1.6$  kcal/mol). Note, however, that the  $|\Delta G^1|$  value for the three calcium reactions (0.7, 1.6, and 0.5 kcal/mol) are smaller than the respective  $|\Delta G^1|$  for the magnesium reactions (1.3, 2.3, and 2.5 kcal/mol), which implies a smaller free-energy penalty for switching between carboxylate-binding modes in Ca sites.

**3.5. Role of the Backbone.** Inner-shell backbone peptide groups or Asn/Gln side chains are often neighbors of the first-shell acidic residues in Ca-binding proteins (see below); thus, Ca complexes with a net charge of +1, 0, and -1, with two water molecules near  $\text{HCOO}^-/\text{HC}\ddot{\text{O}}\ddot{\text{O}}^-$  replaced by  $\text{CH}_3\text{-CONHCH}_3$ , were modeled (see Figures 9 and 10). Unfortunately, thermodynamic parameters for  $[\text{Ca}(\text{H}_2\text{O})_4(\text{CH}_3\text{-CONHCH}_3)_2\text{HCOO}]^+ \rightarrow \{[\text{Ca}(\text{H}_2\text{O})_3(\text{CH}_3\text{-CONHCH}_3)_2\text{HC}\ddot{\text{O}}\ddot{\text{O}}\cdot\text{H}_2\text{O}]^+\}$  could not be obtained, because all the different starting geometries with  $\text{HCOO}^-$  monodentately bound to the Ca(II) cation (see Figure 9a) resulted in a bidentate structure (see Figure 9b) after several steps of optimization.

Nevertheless, the results in Figure 10 show that the water  $\rightarrow$  backbone substitution, which deprives the monodentate structure of favorable hydrogen-bond interactions, favors the bidentate structure enthalpically (the  $\Delta H^1$  values for the neutral and anionic complexes are  $-6.6$  and  $-3.0$  kcal/mol, respectively). In contrast, hydrogen-bonding interactions between the metal-free carboxylate O atoms and neighboring water H atoms in the water/formate complexes (where the two  $\text{CH}_3\text{-CONHCH}_3$  ligands in Figure 10 are replaced by water molecules) energetically stabilize the monodentate structures (the  $\Delta H^1$  value for the neutral and anionic complexes are 2.3 and 3.3 kcal/mol, respectively; see Figure 8). This again emphasizes the role of water in stabilizing the monodentate structure.

**3.6. Effect of Dielectric Medium.** To assess how the relative solvent exposure of the metal-binding site affects the carboxy-

late-binding mode, free energies were evaluated for a series of monodentate/bidentate isomerization reactions in various media, modeled by a dielectric constant of  $\epsilon = 2-80$ , representing metal sites of varying degrees of solvent exposure. Solvation effects do not alter the preferred carboxylate mode that is found in the gas phase (see Table 3). The isomerization free energy remains negative throughout the entire dielectric range studied for Mg(II) and Ca(II) single-formate complexes (see Table 3, reactions 1 and 4). Solvation seems to further stabilize the bidentate carboxylate mode in these cationic complexes (see Table 3; the  $\Delta G^x$  value for reactions 1 and 4 becomes more negative as  $\epsilon$  increases). On the other hand, for neutral/anionic Mg and Ca complexes in which the metal is bound to more than one carboxylate group, the isomerization free energies are positive in both gas-phase and condensed media. Higher solvent accessibility of such binding sites may enhance the preference for the monodentate carboxylate-binding mode. Note that the actual dielectric constant that represents the effect of the protein environment, which is still a debatable issue,<sup>61,62</sup> would not affect the aforementioned conclusions, based on the trend/sign of the free-energy change (as opposed to the absolute free energy) for a given reaction, which remains the same throughout the entire dielectric range from  $\epsilon = 1$  to  $\epsilon = 80$  (see Table 3).

**3.7. Carboxylate-Binding Mode in Protein Mg- and Ca-Binding Sites.** The PDB search (see Methods section) resulted in 27 Mg(II)- and 54 Ca(II)-binding sites that contained Asp/Glu ligands in the metal inner coordination shell. The number of Asp/Glu residues per binding site in Ca(II) proteins was determined to be 2.5, whereas the respective number for Mg(II)-binding sites is 2.0. However, the ratio between monodentately and bidentately bound carboxylates in the two groups of proteins differs significantly. There is only one Mg(II)-binding site (in human phosphatase, PDB entry 1EW2) where a Glu binds the metal in a bidentate fashion (accounting for 4% of the cases), whereas almost one-third (29%) of the acidic side chains in Ca(II) proteins prefer bidentate binding (Figure 11a).

Another difference between Mg- and Ca-binding sites is the frequency distributions of neutral water and backbone ligands. Water ligands are approximately twice as abundant in Mg sites (3.2 water molecules per binding site, or 54% of the total number of the first-shell ligands; see Figure 11b), compared to Ca sites (1.5 water molecules per binding site, or 24% of the first-shell ligands), whereas backbone peptide groups or Asn/Gln side chains are scarce in Mg sites (0.4 per binding site; 6% of the first-shell ligands) but common in Ca-binding sites (1.9 per binding site; 31% of the first-shell ligands). These findings imply that the different architecture of the Mg(II)- and Ca(II)-binding sites, which results in different interligand interactions, might be linked to the observed variations in carboxylate-binding geometries (see below).

## 4. Discussion

**4.1. Comparison with Experiment.** Calculated metal cation-carboxylate O atom distances are reasonably close to the respective experimentally observed values. The calculated average Mg-O(COO) bond distance in the monodentate complexes is  $2.06 \text{ \AA}$ , whereas the respective experimental bond length from the PDB structures is  $2.13 \text{ \AA}$ . The computed average Ca-O bond distances in the monodentate and bidentate structures are  $2.43$  and  $2.49 \text{ \AA}$ , respectively, which also compare well with those in proteins ( $2.37$  and  $2.53 \text{ \AA}$ , respectively). The observed discrepancy between the computed and X-ray metal-O(COO) bond distances may be partly because the former correspond to gas-phase structures.



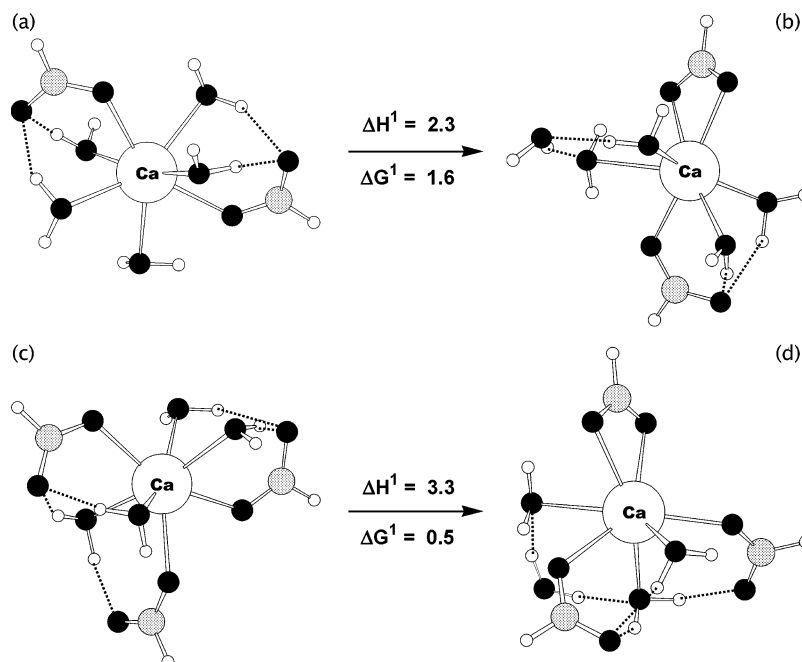


**Figure 8.** Ball-and-stick diagrams of the fully optimized complexes (a)  $[\text{Ca}(\text{H}_2\text{O})_5(\text{HCOO})_2]^0$ , (b)  $\{[\text{Ca}(\text{H}_2\text{O})_4(\text{HCOO})\text{HCOO}]\cdot\text{H}_2\text{O}\}^0$ , (c)  $[\text{Ca}(\text{H}_2\text{O})_4(\text{HCOO})_3]^-$ , and (d)  $\{[\text{Ca}(\text{H}_2\text{O})_3(\text{HCOO})_2\text{HCOO}]\cdot\text{H}_2\text{O}\}^-$ . Gas-phase enthalpies ( $\Delta H^1$ ) and free energies ( $\Delta G^1$ ) are given in kcal/mol.

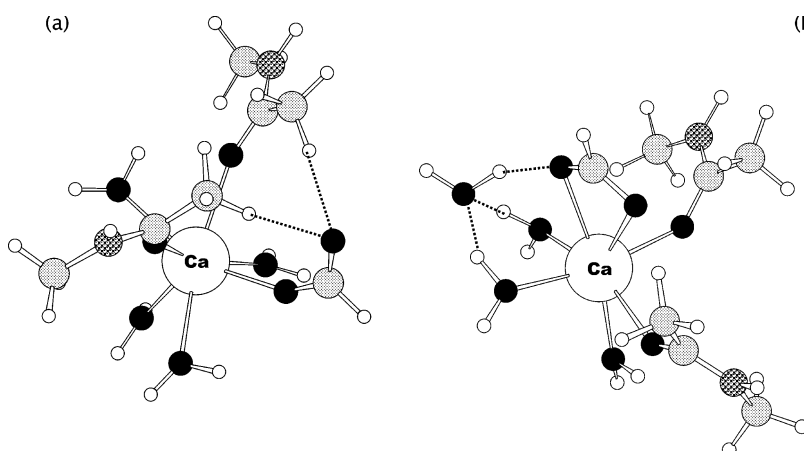


**Figure 9.** Ball-and-stick diagrams of the (a) initial and (b) final structure of the  $[\text{Ca}(\text{H}_2\text{O})_4(\text{CH}_3\text{CONHCH}_3)_2\text{HCOO}]^+$  complex.

The preferred carboxylate-binding mode in Mg/Ca complexes predicted by the calculations is in accord with that observed in PDB structures that contain metal-binding sites of the same first-shell composition and relative solvent accessibility. Mg-binding sites in X-ray structures are relatively buried with a high ratio of water:backbone ligand (see Figure 11). In a water-rich octahedral Mg(II) complex that contains five water molecules and a single carboxylate, the bidentate mode is slightly more favorable than the monodentate one (see Figure 1a and b; a negative  $\Delta G$  value is observed for reaction 1 in Table 3); however, because of the small  $|\Delta G|$  value ( $-1.5$  to  $-2.3$  kcal/mol), additional second-shell interactions that stabilize the metal-free carboxylate O atom could favor the monodentate structure (see Results section). This finding is consistent with PDB structures of the same first-shell arrangement where Asp/Glu binds Mg(II) bidentately in the absence of second-shell interactions, stabilizing the metal-free carboxylate O atom, but it binds Mg(II) monodentately when the monodentate carboxylate, which forms a “hydrogen-bonded motif” with a first-shell water molecule, is additionally stabilized by interactions with second-shell ligands, such as a water molecule [casein kinase II (1QF8)], or a pair of a backbone amide and a water [Udp-glucosyltrans-

ferase (1IIR)], or an asparagine side chain and a water [porphobilinogen synthase (1I8J)]. When the Mg(II) cation is octahedrally bound to more than one carboxylate ligand and at least three water molecules, it prefers to bind monodentately to all the carboxylate groups, which are stabilized by favorable hydrogen-bonding interactions with the first-shell water molecules (positive  $\Delta G$  value for reactions 2 and 3 in Table 3) and/or second-shell protein/water ligands. Crystal structures of Mg-binding sites in proteins with the same first-shell composition confirm that this is indeed the case: X-ray structures of Mg-binding sites with the Mg(II) cation hexacoordinated to two Asp/Glu [ASV integrase (1VSD), decarboxylase (1KV8) and synthase (1N1B)], or three Asp/Glu [enolase (1EBH), epimerase (1JPM) and beta-methyl aspartase (1KCZ)] show all the Asp/Glu monodentately bound to the Mg(II) cation.

In contrast to the Mg-binding sites, many Ca-binding sites in X-ray structures have a higher ratio of backbone:water ligand (see Figure 11b). In Ca complexes with two backbone ligands, the bidentate carboxylate mode seems to be more stable than the corresponding monodentate carboxylate mode, as evidenced by the negative  $\Delta G^1$  value in Figure 10. This finding is consistent with X-ray structures of Ca-binding sites with Ca-

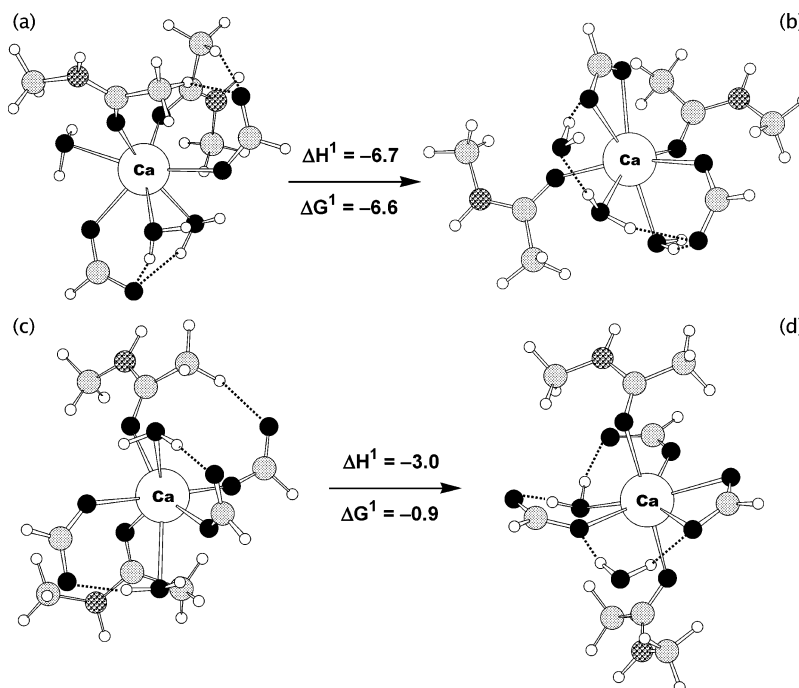


**Figure 10.** Ball-and-stick diagrams of (a)  $[\text{Ca}(\text{H}_2\text{O})_3(\text{CH}_3\text{CONHCH}_3)_2(\text{HCOO})_2]^0$ , (b)  $\{[\text{Ca}(\text{H}_2\text{O})_2(\text{CH}_3\text{CONHCH}_3)_2(\text{HCOO})\text{HC}\ddot{\text{O}}\ddot{\text{O}}]\cdot\text{H}_2\text{O}\}^0$ , (c)  $[\text{Ca}(\text{H}_2\text{O})_2(\text{CH}_3\text{CONHCH}_3)_2(\text{HCOO})_3]^-$ , and (d)  $\{[\text{Ca}(\text{H}_2\text{O})(\text{CH}_3\text{CONHCH}_3)_2(\text{HCOO})_2\text{HC}\ddot{\text{O}}\ddot{\text{O}}]\cdot\text{H}_2\text{O}\}^-$ . Gas-phase enthalpies ( $\Delta H^1$ ) and free energies ( $\Delta G^1$ ) are given in kcal/mol.

**TABLE 3: Free Energies ( $\Delta G^x$ ) for Monodentate–Bidentate Carboxylate Isomerization in Mg(II) and Ca(II) Water (W)–Formate Complexes Evaluated for Different Dielectric Media with  $\epsilon = x$  ( $x = 1, 2, 4, 10$ , and 80)**

reaction	Free Energy (kcal/mol)				
	$\Delta G^1$	$\Delta G^2$	$\Delta G^4$	$\Delta G^{10}$	$\Delta G^{80}$
1 $[\text{MgW}_3\text{HCOO}]^+ \rightarrow \{[\text{MgW}_4\text{HC}\ddot{\text{O}}\ddot{\text{O}}]\cdot\text{W}\}^+$	-1.3	-1.5	-1.8	-2.1	-2.3
2 $[\text{MgW}_4(\text{HCOO})_2]^0 \rightarrow \{[\text{MgW}_3(\text{HCOO})\text{HC}\ddot{\text{O}}\ddot{\text{O}}]\cdot\text{W}\}^0$	2.3	2.3	2.3	2.4	2.7
3 $[\text{MgW}_3(\text{HCOO})_3]^- \rightarrow \{[\text{MgW}_2(\text{HCOO})_2\text{HC}\ddot{\text{O}}\ddot{\text{O}}]\cdot\text{W}\}^-$	2.5	2.7	2.8	3.0	3.3
4 $[\text{CaW}_6\text{HCOO}]^+ \rightarrow \{[\text{CaW}_5\text{HC}\ddot{\text{O}}\ddot{\text{O}}]\cdot\text{W}\}^+$	-0.7	-1.7	-2.4	-2.9	-3.3
5 $[\text{CaW}_5(\text{HCOO})_2]^0 \rightarrow \{[\text{CaW}_4(\text{HCOO})\text{HC}\ddot{\text{O}}\ddot{\text{O}}]\cdot\text{W}\}^0$	1.6	1.6	1.8	2.2	2.5
6 $[\text{CaW}_4(\text{HCOO})_3]^- \rightarrow \{[\text{CaW}_3(\text{HCOO})_2\text{HC}\ddot{\text{O}}\ddot{\text{O}}]\cdot\text{W}\}^-$	0.5	1.1	1.7	2.1	2.3

(II) heptacoordinated to two backbone groups/Asn/Gln, two Asp/Glu and two water molecules [calpain 1ALV (site 1), thermitase 1THM (site 2) and stromelysin-1 1HY7 (site 1)], or two backbone groups/Asn/Gln, three Asp/Glu and one water [MRP14 1IRJ (site 1), sarcoplasmic calcium-binding protein 2SCP (sites 2 and 3), sparc 1SRA (site 1), recoverin 1REC, calmodulin 1OSA (sites 2 and 3) and isoamylase (1BF2)], which show one of the acidic residues bidentately bound to the Ca(II) cation.

The finding here, that bidentate carboxylate binding is favored in larger metal complexes with higher CNs, is also consistent with previous statistical surveys of X-ray structures in the CSD. The percentage of bidentately bound carboxylates increases as the CN of the metal increases: values of 0%, 16%, and 25% are observed for hexa-, hepta- and octacoordinated Ca clusters, respectively.<sup>39</sup>

#### 4.2. Factors Determining the Carboxylate-Binding Mode.

The results show that a key factor in determining the carboxylate-binding mode is the availability and type of interactions between the metal-free carboxylate O atom and its neighbors. In the absence of such interligand interactions, the bidentate carboxylate mode is inherently more stable than its monodentate counterpart, although the energy difference between the two is relatively small. Very often, however, the monodentate carboxylate is engaged via its metal-free O atom in various interactions with neighboring inner or outer-shell metal ligands. These, depending on their strength, may overcome the energy difference between the monodentate and bidentate structures,

thus making the monodentate geometry more favorable than the respective bidentate one. For example, if water molecules hydrogen-bond to the metal-free carboxylate O atom, monodentate carboxylate binding is preferred over the bidentate mode in Ca(II) water–formate complexes with an overall charge of 0 (see Figure 8). On the other hand, if weaker hydrogen-bond acceptors, such as  $\text{CH}_3\text{CONHCH}_3$ , interact with the metal-free carboxylate O atom, bidentate neutral complexes remain dominant (see Figure 10). Some monodentate structures where the metal-free carboxylate O atom lacks appropriate interactions with its neighbors (e.g., Figure 2a or 9a) were found to be unstable, relative to the respective bidentate structures.

Another factor that governs the carboxylate-binding mode is the interactions between the carboxylate O atoms and the metal cation itself. Cations that can accept more charge from both carboxylate O centers, relative to a single carboxylate O atom, favor bidentate carboxylate binding. In the series of Zn(II), Mg(II), and Ca(II) water–formate complexes in Table 1, zinc can accept more charge from both carboxylate O centers, relative to a carboxylate O atom than the Mg(II) and Ca(II) cations; therefore, it stabilizes the bidentate formate to a greater extent than the other two cations. Increasing the metal coordination number upon carboxylate binding favors the bidentate mode. In the series of Zn(II) and Ca(II) water–formate complexes in Figures 3 and 4, the complexes with higher CN (and, thus, greater steric repulsion among the ligands) are more stable with

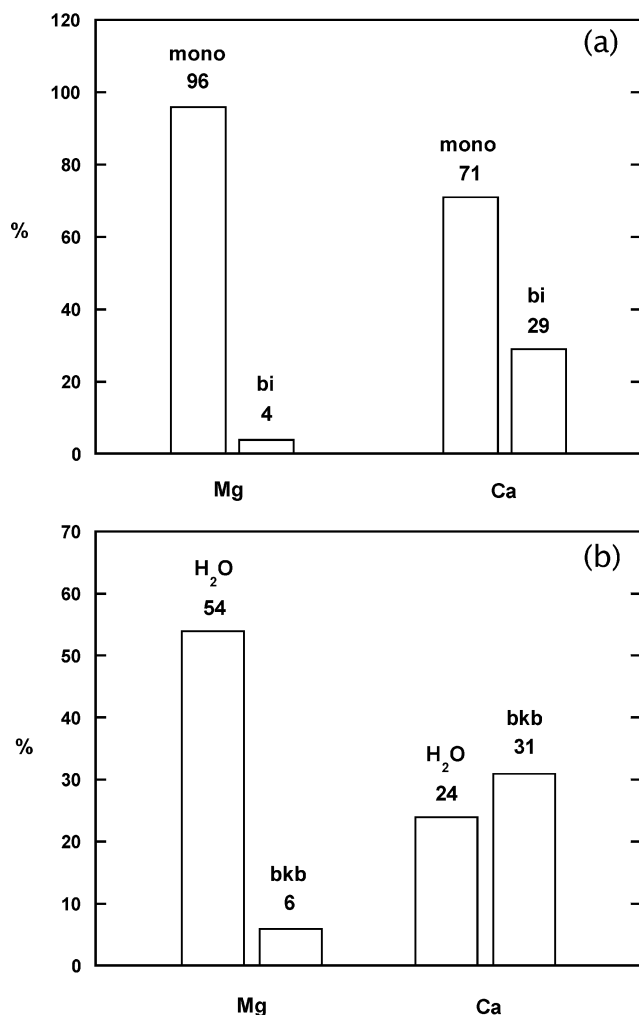


**Figure 11.** Percentage frequency distribution of (a) monodentate (mono) and bidentate (bi) carboxylate side chains and (b) water (H<sub>2</sub>O) and backbone (bkb) found in three-dimensional PDB structures of magnesium and calcium proteins.

the less-space-demanding bidentate HCO<sup>-</sup> than with the hydrogen-bonded monodentate motif, HCOO<sup>-</sup>...H<sub>2</sub>O.

The metal size also indirectly influences the carboxylate-binding mode. For two metals with the same CN and similar charge-accepting ability, the smaller metal favors monodentate carboxylate binding, because it prefers binding to water molecules (as opposed to bulky protein main chain/side chain dipoles), which can hydrogen-bond to the metal-free carboxylate O atoms. Therefore, because the Mg(II) cation is much smaller than the Ca(II) cation (the ionic radii of hexacoordinated Mg(II) and Ca(II) are 0.72 and 1.00 Å, respectively<sup>63</sup>), it is harder to solvate Mg-carboxylate complexes with bulky protein main chain/side chain dipoles than the respective Ca-carboxylate complexes.<sup>60</sup> Consequently, Mg-carboxylate complexes are better hydrated than the respective Ca-carboxylate complexes, as found in Figure 11b, and prefer monodentate carboxylate binding, as observed in Figure 11a, because of favorable HCOO<sup>-</sup>...H<sub>2</sub>O hydrogen-bonding interactions. However, when the partial positive charge on the metal is reduced by incorporating more negatively charged ligands into the complex, the role of direct metal-carboxylate interactions in determining the carboxylate-binding mode diminishes, thus giving more weight to other factors, such as first/second-shell ligand-carboxylate interactions, in determining the carboxylate-binding mode.

**4.3. Biological Implications.** Altogether, the aforementioned theoretical results imply that the carboxylate-binding mode is

determined by competition between the metal cation, on one hand, and nonacidic neighboring ligands from the metal inner or outer coordination sphere, on the other, for the second O atom of the COO<sup>-</sup> moiety. When the positive charge of the metal is reduced by coordination to negatively charged ligands, first- or second-shell ligand-carboxylate (as opposed to direct metal-carboxylate) interactions dictate the carboxylate-binding mode. In such cases, where the metal is bound to more than one carboxylate group, water molecules have a crucial role in stabilizing the monodentate carboxylate-binding mode of water-rich Mg complexes, whereas the peptide backbone has a role in destabilizing the monodentate carboxylate-binding mode of the “drier” and bulkier Ca complexes. Thus, by fine-tuning the respective interactions, the protein can adopt an appropriate binding site configuration.

**Acknowledgment.** We thank Dr. J. Wright for writing the program to analyze the metal-binding sites from the Protein Data Bank (PDB). We are grateful to D. Bashford, M. Sommer, and M. Karplus for the program to solve the Poisson equation. This work was supported by the National Science Council, Taiwan (under NSC Contract No. 91-2311-B-001), the Institute of Biomedical Sciences, and the National Center for High-Performance Computing, Taiwan.

## References and Notes

- (1) Bertini, I.; Sigel, A.; Sigel, H., Eds. *Handbook on Metalloproteins*; Marcel Dekker: New York, 2001.
- (2) Jernigan, R.; Raghunathan, G.; Bahar, I. *Curr. Opin. Struct. Biol.* **1994**, *4*, 256.
- (3) Dudev, T.; Lin, Y. L.; Dudev, M.; Lim, C. *J. Am. Chem. Soc.* **2003**, *125*, 3168.
- (4) Dudev, T.; Cowan, J. A.; Lim, C. *J. Am. Chem. Soc.* **1999**, *121*, 7665.
- (5) Casareno, R. L. B.; Li, D.; Cowan, J. A. *J. Am. Chem. Soc.* **1995**, *117*, 11011.
- (6) Dismukes, G. C. *Chem. Rev.* **1996**, *96*, 2909.
- (7) Christianson, D. W. *Adv. Protein Chem.* **1991**, *42*, 281.
- (8) Christianson, D. W.; Cox, J. D. *Annu. Rev. Biochem.* **1999**, *68*, 33.
- (9) Vallee, B. L.; Auld, D. S. *Biochemistry* **1990**, *29*, 5647.
- (10) Pidcock, E.; Moore, G. R. *J. Biol. Inorg. Chem.* **2001**, *6*, 479.
- (11) Bock, C. W.; Katz, A. K.; Markham, G. D.; Glusker, J. P. *J. Am. Chem. Soc.* **1999**, *121*, 7360.
- (12) Lipscomb, W. N.; Strater, N. *Chem. Rev.* **1996**, *96*, 2375.
- (13) Coleman, J. E. *Annu. Rev. Biochem.* **1992**, *61*, 897.
- (14) Alberts, I. L.; Nadassy, K.; Wodak, S. J. *Protein Sci.* **1998**, *7*, 1700.
- (15) Bertini, I.; Gray, H. B.; Lippard, S. J.; Valentine, J. S. *Bioinorganic Chemistry*; University Science Books: Mill Valley, CA, 1994.
- (16) Rulisek, L.; Vondrasek, J. *J. Inorg. Biochem.* **1998**, *71*, 115.
- (17) Dudev, T.; Lim, C. *Chem. Rev.* **2003**, *103*, 773.
- (18) Garmer, D. R.; Gresh, N. *J. Am. Chem. Soc.* **1994**, *116*, 3556.
- (19) Mercero, J. M.; Fowler, J. E.; Ugalde, J. M. *J. Phys. Chem. A* **1998**, *102*, 7006.
- (20) Mercero, J. M.; Fowler, J. E.; Ugalde, J. M. *J. Phys. Chem. A* **2000**, *104*, 7053.
- (21) Rulisek, L.; Havlas, Z. *J. Am. Chem. Soc.* **2000**, *122*, 10428.
- (22) Rulisek, L.; Havlas, Z. *J. Phys. Chem. A* **2002**, *106*, 3855.
- (23) Mercero, J. M.; Matxain, J. M.; Lopez, X.; Fowler, J. E.; Ugalde, J. M. *Int. J. Quantum Chem.* **2002**, *90*, 859.
- (24) Falke, J. J.; Drake, S. K.; Hazard, A. L.; Peersen, O. B. *Q. Rev. Biophys.* **1994**, *27*, 219.
- (25) Drake, S. K.; Lee, K. L.; Falke, J. J. *Biochemistry* **1996**, *35*, 6697.
- (26) Drake, S. K.; Zimmer, M. A.; Kundrot, C.; Falke, J. J. *J. Gen. Physiol.* **1997**, *110*, 173.
- (27) Drake, S. K.; Zimmer, M. A.; Miller, C. L.; Falke, J. J. *Biochemistry* **1997**, *36*, 9917.
- (28) Bourret, R. B.; Hess, J. F.; Simon, M. I. *Proc. Natl. Acad. Sci. U.S.A.* **1990**, *87*, 41.
- (29) Drake, S. K.; Bourret, R. B.; Luck, L. A.; Simon, M. I.; Falke, J. J. *J. Biol. Chem.* **1993**, *268*, 13081.
- (30) Rardin, R. L.; Tolmann, W. B.; Lippard, S. J. *New J. Chem.* **1991**, *15*, 417.
- (31) Gagne, S. M.; Li, M. X.; Sykes, B. D. *Biochemistry* **1997**, *36*, 4386.

- (32) Ozawa, T.; Fukuda, M.; Nara, M.; Nakamura, A.; Komine, Y.; Kohama, K.; Umezawa, Y. *Biochemistry* **2000**, *39*, 14495.
- (33) Babu, C. S.; Dudev, T.; Casareno, R.; Cowan, J. A.; Lim, C. J. *Am. Chem. Soc.* **2003**, *125*, 9318.
- (34) Allen, F. H. *Acta Crystallogr., Sect. B: Struct. Sci.* **2002**, *B58*, 380.
- (35) Bernstein, F. C.; Koetzle, T. F.; Williams, G. J. B.; Meyer, E. F.; Brice, M. D.; Rodgers, J. R.; Kennard, O.; Shimanouchi, T.; Tasumi, M. *J. Mol. Biol.* **1977**, *122*, 535.
- (36) Einspahr, H.; Bugg, C. E. In *Metal Ions in Biological Systems*; Sigel, H., Ed.; Marcel Dekker: Basel, Switzerland, 1984; Vol. 17, p 51.
- (37) Carrell, C. J.; Carrell, H. L.; Erlebach, J.; Glusker, J. P. *J. Am. Chem. Soc.* **1988**, *110*, 8651.
- (38) Chakrabarti, P. *Protein Eng.* **1990**, *4*, 49.
- (39) Katz, A. K.; Glusker, J. P.; Beebe, S. A.; Bock, C. W. *J. Am. Chem. Soc.* **1996**, *118*, 5752.
- (40) Harding, M. M. *Acta Crystallogr., Sect. D: Biol. Crystallogr.* **1999**, *D55*, 1432.
- (41) Ryde, U. *Biophys. J.* **1999**, *77*, 2777.
- (42) Tiraboschi, G.; Roques, B.-P.; Gresh, N. *J. Comput. Chem.* **1999**, *20*, 1379.
- (43) Cini, R. *J. Biomol. Struct. Dyn.* **1999**, *16*, 1225.
- (44) Becke, A. D. *J. Chem. Phys.* **1993**, *98*, 5648.
- (45) Lee, C.; Yang, W.; Parr, R. G. *Phys. Rev. B* **1988**, *B37*, 785.
- (46) Dudev, T.; Lim, C. *J. Am. Chem. Soc.* **2000**, *122*, 11146.
- (47) Dudev, T.; Lim, C. *J. Phys. Chem. B* **2001**, *105*, 4446.
- (48) Dudev, T.; Lim, C. *J. Phys. Chem. B* **2001**, *105*, 10709.
- (49) Frisch, M. J.; Trucks, G. W.; Schlegel, H. B.; Scuseria, G. E.; Robb, M. A.; Cheeseman, J. R.; Zakrzewski, V. G.; Montgomery, J. A., Jr.; Stratmann, R. E.; Burant, J. C.; Dapprich, S.; Millam, J. M.; Daniels, A. D.; Kudin, K. N.; Strain, M. C.; Farkas, O.; Tomasi, J.; Barone, V.; Cossi, M.; Cammi, R.; Mennucci, B.; Pomelli, C.; Adamo, C.; Clifford, S.; Ochterski, J.; Petersson, G. A.; Ayala, P. Y.; Cui, Q.; Morokuma, K.; Malick, D. K.; Rabuck, A. D.; Raghavachari, K.; Foresman, J. B.; Cioslowski, J.; Ortiz, J. V.; Stefanov, B. B.; Liu, G.; Liashenko, A.; Piskorz, P.; Komaromi, I.; Gomperts, R.; Martin, R. L.; Fox, D. J.; Keith, T.; Al-Laham, M. A.; Peng, C. Y.; Nanayakkara, A.; Gonzalez, C.; Challacombe, M.; Gill, P. M. W.; Johnson, B. G.; Chen, W.; Wong, M. W.; Andres, J. L.; Head-Gordon, M.; Replogle, E. S.; Pople, J. A. *Gaussian 98*, revision A.5; Gaussian, Inc.: Pittsburgh, PA, 1998.
- (50) Wong, M. W. *Chem. Phys. Lett.* **1996**, *256*, 391.
- (51) McQuarrie, D. A. *Statistical Mechanics*; Harper and Row: New York, 1976.
- (52) Gilson, M. K.; Honig, B. *Biopolymers* **1986**, *25*, 2097.
- (53) Lim, C.; Bashford, D.; Karplus, M. *J. Phys. Chem.* **1991**, *95*, 5610.
- (54) MacKerell, J. A. D.; Bashford, D.; Bellott, M.; Dunbrack, R.; Evanseck, J. D.; Field, M. J.; Fischer, S.; Gao, J.; Guo, H.; Ha, S.; Joseph-McCarthy, D.; Kuchnir, L.; Kuczera, K.; Lau, F. T. K.; Mattos, C.; Michnick, S.; Ngo, T.; Nguyen, D. T.; Prodhom, B.; Reiher, W. E. I.; Roux, B.; Schlenkrich, M.; Smith, J. C.; Stote, R.; Straub, J.; Watanabe, M.; Wiorkiewicz-Kuczera, J.; Yin, D.; Karplus, M. *J. Phys. Chem. B* **1998**, *102*, 3586.
- (55) Dudev, T.; Lim, C. *J. Phys. Chem. B* **2000**, *104*, 3692.
- (56) Reed, A. E.; Curtiss, L. A.; Weinhold, F. *Chem. Rev.* **1988**, *88*, 899.
- (57) Sali, A.; Blundell, T. L. *J. Mol. Biol.* **1993**, *234*, 779.
- (58) Katz, A. K.; Glusker, J. P.; Markham, G. D.; Bock, C. W. *J. Phys. Chem. B* **1998**, *102*, 6342.
- (59) Chang, L.-Y.; Lim, C. manuscript in preparation.
- (60) Dudev, T.; Lim, C. *J. Phys. Chem. A* **1999**, *103*, 8093.
- (61) Mertz, E. L.; Krishtalik, L. I. *Proc. Natl. Acad. Sci. U.S.A.* **2000**, *97*, 2081.
- (62) Schutz, C. N.; Warshel, A. *Proteins: Struct., Funct., Genet.* **2001**, *44*, 400.
- (63) Marcus, Y. *Chem. Rev.* **1988**, *88*, 1475.